

We are IntechOpen, the world's leading publisher of Open Access books Built by scientists, for scientists

6,900

Open access books available

186,000

International authors and editors

200M

Downloads

Our authors are among the

154

Countries delivered to

TOP 1%

most cited scientists

12.2%

Contributors from top 500 universities



WEB OF SCIENCE™

Selection of our books indexed in the Book Citation Index
in Web of Science™ Core Collection (BKCI)

Interested in publishing with us?
Contact book.department@intechopen.com

Numbers displayed above are based on latest data collected.
For more information visit www.intechopen.com



Capillary Driven Flows under Microgravity Conditions: From Parabolic Flights to Space Experiment

*Nikolay Smirnov, Valeriy Nikitin
and Evgeniya Kolenkina (Skryleva)*

Abstract

The chapter investigates imbibition into a porous medium under microgravity condition under the action of capillary forces. The study of capillary effects in terrestrial conditions is often difficult due to the influence of gravity, which makes it necessary to conduct experiments in microgravity. The chapter describes the features of experiments and the processing of experimental data in two types of microgravity experiments: during parabolic flights and at space stations in terrestrial orbit. During parabolic flights, a highly permeable artificial porous medium consisting of glass balls of the same size was considered (such a medium makes it easy to visualize experimental results and simulate media with different permeability using balls of different diameters). In experiments in orbit, the flow of fluids with various physical properties in natural sands was considered. The chapter also describes the mathematical modeling of such processes and presents the results of numerical simulations and their comparison with experimental data. The possibility of determining rheological relationships for capillary forces being functions of governing parameters in porous medium on the basis of data obtained from experiments in microgravity is demonstrated.

Keywords: microgravity, imbibition, parabolic flights, porous medium, capillary effects

1. Introduction

Investigation of capillary driven seepage under microgravity conditions is of great interest for space applications and terrestrial engineering and technology. On space platforms, capillary transport of liquids is observed in various devices/processes such as purification filtration systems, heat pipes, and fuel transport from tanks in weightlessness. Capillary forces turn to be the major mechanism driving the feeding fluid to the plant's roots in hydroponics plant growth systems in space.

On the other hand, microgravity investigation of seepage processes gives a deeper insight in the fundamentals of this nonequilibrium phenomenon, thus providing a better understanding of seepage processes for terrestrial applications, such as oil recovery. Microgravity conditions allow us to study capillary effects in large

pores, which are impossible in terrestrial conditions due to the influence of gravity, which distorts the shape of the interface and changes effects.

Under terrestrial conditions, the capillary forces are partly shielded by gravity effects, but, nevertheless, are still present. Accurate investigation of wettability effects in immiscible fluids filtration requires abandoning all other effects as far as possible. Determination of some rheological relationships for accounting the influence of capillary forces in porous media is possible by performing experiments under reduced gravity conditions. Such relationships can then be introduced into already existing models, integrating heat and mass transfer through porous media.

The process of imbibition of viscous fluids into a porous medium depends essentially on capillary effects and instability, which may develop on the displacement front in case of multiphase flow. Accounting for capillary forces is critical for the description of the motion of liquids in porous media. The study of the capillary effects under ordinary conditions is difficult because of the significant effect of gravity on the seepage process in big pores, wherein visual registration is possible. Therefore, in this chapter, we consider the flow of liquids in a porous medium under microgravity conditions during parabolic flights. The problem of multiphase seepage in porous media is very well developed. There is a lot of different models based on the modified Darcy law [1–6]. Experimental and theoretical studies of the flow of fluids in porous media and natural sands under microgravity conditions have been carried out, and mathematical models describing these processes have been developed [7–11]. Another important factor, which influences the displacement, is the instability developing at the front. Initially flat interface of the liquids is broken; some “fingers” of the liquid break through, which causes liquid being entrapped inside the porous medium. The unstable liquid displacement is well studied [12, 13]. Experiments on the flow of liquids through a porous medium under microgravity conditions under the action of capillary forces are described in [9]. The motivation for the present study is investigating the flow of fluid in an artificial porous medium containing heterogeneities under the action of capillary forces. Professor Jean-Claude Legros (**Figure 1**) and his student Eric Istasse were engaged in the determination of capillary characteristics in porous media, and they



Figure 1.
Professor Jean Claude Legros (left) with Professor Nikolay Smirnov (right).

conducted experiments on imbibition of fluids into porous media during parabolic flights. In this chapter, the results of these experiments are reviewed and compared with the results of numerical simulation. In the case of a porous medium formed by relatively large particles, it becomes important to take into account additional inner terms in the Darcy equation. The corresponding mathematical model is described here. Models without inertia effects, described in detail in [2–4], describe fairly accurately slow flows in classical low-permeable porous media, but they are not suitable for processes discussed here.

In this chapter, we focus on seepage flows in porous media with inhomogeneity. The presence of heterogeneity brings to the nonuniformity of the seepage flow and the displacement front, which can lead to nonlinear physical results. Such nonlinear physical results are described in detail in [14], where experiments on the imbibition of liquids into a natural porous medium under microgravity conditions are considered. Results showed that a point located higher along the length of a sample can be reached by a liquid faster than a lower one. In a natural porous medium, we can only make hypothesis about the reasons of such a behavior; while using an artificial porous medium assembled of transparent glass balls, one can visually register the effect of heterogeneity on the capillary driven seepage flow.

2. Experimental investigations imbibition into artificial porous medium

Parabolic flight campaigns were organized (and funded) by the European Space Agency. The parabolic flights are achieved using the French Airbus A300-ZeroG, an aircraft especially transformed to a rather big microgravity laboratory. Detailed description of experimental procedures and techniques can be found in [15]. Below we provide a shortened version of the description.

Microgravity conditions encountered during the parabolic flight exercise are very special ones, and anybody will certainly understand that they are far from usual ground-based laboratory conditions. The design of a dedicated experimental payload must thus integrate the specific aspects of reduced gravity environment. For example, flight procedures should be simplified as much as possible, rendering in-flight operations easy to perform. Mass and overall dimensions of the experimental setup are also limiting factors that have to be carefully considered during the payload design.

A typical parabolic flight campaign is usually scheduled around three successive flights days, preceded by 10 days of experiment integration and eventual “last minute” modifications. The short period of time between the flight opportunities may impact the intrinsic conception of the experimental devices, e.g., experimental cells, payload maintenance tasks, and so on. Furthermore, the aircraft safety rules are very strict, and any boarding experiment must first pass a detailed control procedure, performed by the safety crewmembers.

All these aspects are part of a weightlessness flight program and have to be kept in mind during the preparation of a flight opportunity.

2.1 Instrumental setup description

Several experimental parameters were fixed before setting the design of the experiment:

- We consider porous samples made of glass spheres having various granulometric size distributions. The regular shape of the glass spheres will eliminate potential anisotropy of the porous sample, simplifying thus the

investigation of the observed flows. Another advantage is the translucent character of the glass spheres that enables us to visualize in some way internal fluid motions that are usually inaccessible by direct visualization. Finally, choosing spherical constituting solid particles makes it possible to realize a lot of different samples with various well-known intrinsic properties, i.e., porosity, permeability, and mean characteristic pore radius. Overall dimensions of the porous samples ($75 \times 50 \times 200 \text{ mm}^3$) have been determined taking into account the available duration of microgravity.

- We investigated several fluid systems. The simplified two-phase flow model, presented in the previous section, is experimentally investigated in the case of a water-air system and in the case of a water-alkane system. We choose the iso-octane, also known as 2,2,4-trimethylpentane, for the hydrocarbon, because it is less dense than water, completely immiscible with it. Iso-octane is less wetting the porous matrix as compared with water. This liquid-liquid system investigation enables us to vary the surface tension parameter without modifying the wettability properties of the porous medium. Furthermore, the viscosity of iso-octane is less than the water one. Hence, we limited the appearing of viscous fingering phenomenon that tends to greatly destabilize the moving liquid-liquid interface. The stable shape of the interface is indeed a necessary condition to neglect the dispersion fluxes appearing in our mathematical model.
- The boundary conditions mentioned for the mathematical model, namely no hydrostatic pressure difference between bottom and top of the porous sample, were satisfied. We have also seen that it is necessary to avoid as far as possible the capillary effects at the level of the fluid reservoir. This was achieved by saturating completely the reservoir with the wetting fluid. Note that this reservoir must be able to deform when the capillary flow occurred in microgravity, otherwise we would have observed the formation of an air bubble, which, if growing, would have been able to block the entrance of the porous sample for the fluid. Hence, the reservoir consisted of a deformable plastic bag that remained full of liquid during flight conditions.
- During the parabola, the transition period between the pull-up phase and the microgravity phase induced undesired effects that greatly influenced the flow through the porous sample. Capillary driven filtration started indeed immediately at the beginning of the transition period. At this particular moment, we did not have clear initial conditions for the subsequent creeping under reduced gravity. Hence, it was very important for the filtration modeling to restrict as much as possible the transient flow occurring during this transition phase. It was preferable to wait for acceptable reduced gravity conditions to start up the flow. The experimental setup incorporated simple technical solutions to control these undesired effects. The hydraulic scheme of the experiment indeed included electromagnetic valves that allowed us to close hermetically the porous medium. Consequently, if a capillary flow was starting during the transition phase, it would be rapidly damped by the air pressure increase, which was resulting from the decrease of the volume accessible for the gaseous phase inside the cell. Once in real microgravity, we simply opened the valves to allow the capillary driven flow to invade the solid matrix.
- The effect of temperature on surface tension and viscosity properties of the fluids was not considered in the present study. The aircraft air-conditioning system maintained the cabin temperature around 25°C during flight operations.

2.2 Payload description

The experimental payload has been completely designed and developed by the scientific and technical teams of the Physical Chemistry Department of the Free University of Brussels. It incorporated all the necessary devices to study various capillary driven flows under reduced gravity conditions, and its basic features will be now briefly detailed.

The payload consisted of two racks integrating the experimental setup (main rack) and the porous samples confined in dedicated experimental cells (storage rack). The main rack included the following:

- An electrical panel, mandatory to interface the experiment with the aircraft power supplies.
- A video system, including black and white video camera and high-quality video recorder.
- A hydraulic scheme, i.e., a network of valves and tubes necessary to handle the eventual fluid feeding of the experimental cells.
- A temperature and pressure acquisition system was loaded and allowed to work autonomously during the flight. Data were simply downloaded after landing.
- A residual g-level data acquisition system, coupled with the video recording system, enabling video incrustation of residual g-level directly through the video signal.

The main rack measured $880 \times 650 \times 1440 \text{ mm}^3$ (length \times width \times height) and integrated in fact two experiments, with a total mass of approximately 300 kg.

The experimental rack was designed to investigate two experimental cells simultaneously. This was a very convenient feature that made it possible to directly correlate two porous samples having different properties under the same microgravity conditions. As the flight planning was organized in 6 sets of 5 successive parabolas, we investigated the experimental cells by pair, and we video recorded 5 successive capillary creeping for them. Longer breaks between two successive sets of parabolas were used to perform the cells exchange.

Following this scientific strategy, we were able to study the influence of the preimbibition of the porous sample. Starting from a completely dry porous medium, the capillary creeping occurred during the first parabola, followed directly by a drainage process during the pull-out phase. The amount of liquid being trapped inside the porous matrix was depending on the surface tension properties of the fluid-fluid pair under investigation. We observed experimentally that the seepage «creepability» parameter Ψ [7, 15] was significantly influenced by the preimbibition. But, once the porous matrix has been imbibed, following successive imbibition was not modifying essentially its microscopic surface state. Successive capillary seepage during a set of parabolas would invade the porous matrix higher and higher, simply because the fluid encountered less resistance in the already preimbibitted zone and the latter tended to increase during successive capillary driven imbibition. The number of operations that experimenters had to perform during the parabola itself was intentionally small. The parabolic flight maneuver, with its succession of hypergravity and low gravity periods, revealed to be physiologically tiring. In these conditions, the experimental procedures should be as

simple as possible to allow the experimenters to anticipate these repetitive gravity variations. For the capillary creeping experiment, the most difficult tasks were the cells exchange, and the fluid management to adjust correctly the initial fluid levels inside for the porous samples. These tasks were executed before the pull-up phases. As we continuously video recorded the experimental cells, the experimenters had only to wait for the optimal reduced gravity level to switch on the electromagnetic valves, thus enabling the flows through the samples.

2.3 Experiment details and results

We concentrate in this section on the peculiarities of seepage flow in a media containing permeability inhomogeneity. The zones of different permeability were arranged in the experimental cells (**Figure 2**) using glass balls of different diameters. Porous samples were hermetically confined inside the experimental cell, whose overall dimensions were $74 \times 50 \times 315 \text{ mm}^3$. Each cell had a separate fluid reservoir made of a deformable plastic bag. The reservoir fluid capacity was sufficient to fill in totally the porous sample. The experimental cell was connected at its bottom side to a cylindrical connector. This connector was 70 mm long and served as a hydraulic junction between the porous sample and the reservoir, filled in with a water-dye mixture. The diameter of the channel zone has been chosen large enough, i.e., 37 mm, to allow reasonable fluid feeding to the porous medium during microgravity periods. During the flight, the capillary driven filtration was video recorded, using a high-quality video equipment. The back-light system allowed to visualize the phase interface separating water and air.

Three experiments are reported here. In all cases, we considered the imbibition of fluid into the porous media that has been prewetted throughout previous parabolas. Zones with different permeability were formed by spheres with diameters of 2 and 6 mm. The artificial porous medium within each zone was composed of glass balls of the same diameter. Thus, the permeability of the porous medium consisting of spheres ($d = 6 \text{ mm}$) was $K_1 = 8.5 \cdot 10^{-9} \text{ m}^2$, while permeability in the low permeable zone ($d = 2 \text{ mm}$) was $K_2 = 2 \cdot 10^{-9} \text{ m}^2$.

In the first experiment, the whole cell was filled with a homogeneous porous medium consisting of glass spheres with a diameter of 6 mm (**Figure 3**). The graph (**Figure 4**) shows the position of the interface as a function of time. By reducing the gravity level, the capillary driven imbibition of fluid into porous sample begins. During the observation period, the interface did not exceed the height of 40 mm.



Figure 2.
The experimental cell for artificial porous medium.

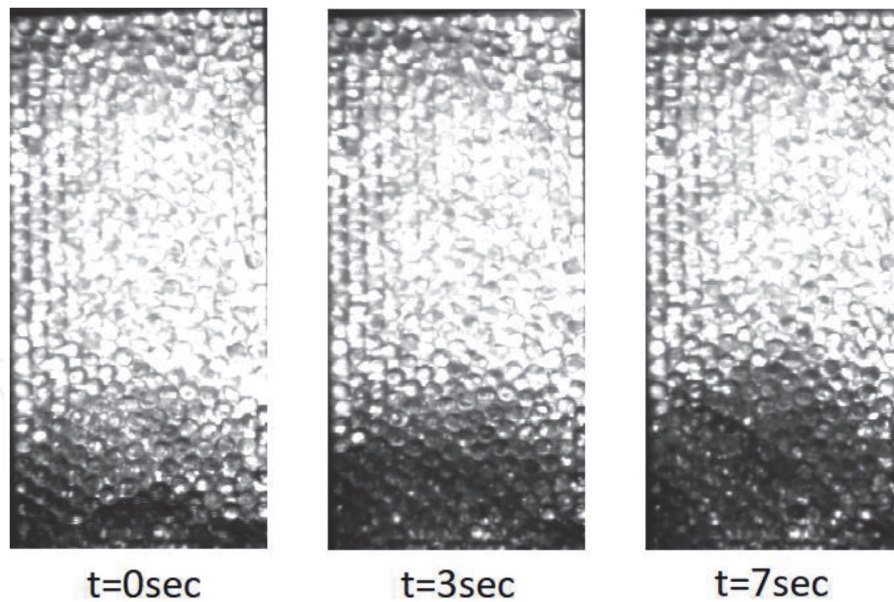


Figure 3.
 The flow of liquid in a porous medium (permeability: $8.5 \cdot 10^{-9} \text{ m}^2$; porosity: 0.458) under microgravity conditions (displacing fluid: viscosity: $1 \cdot 10^{-3} \text{ Pa}\cdot\text{s}$, density: 10^3 kg/m^3 ; displaced gas: viscosity: $1.5 \cdot 10^{-5} \text{ Pa}\cdot\text{s}$, density: 1.4 kg/m^3 ; surface tension: 0.0582 N/m).

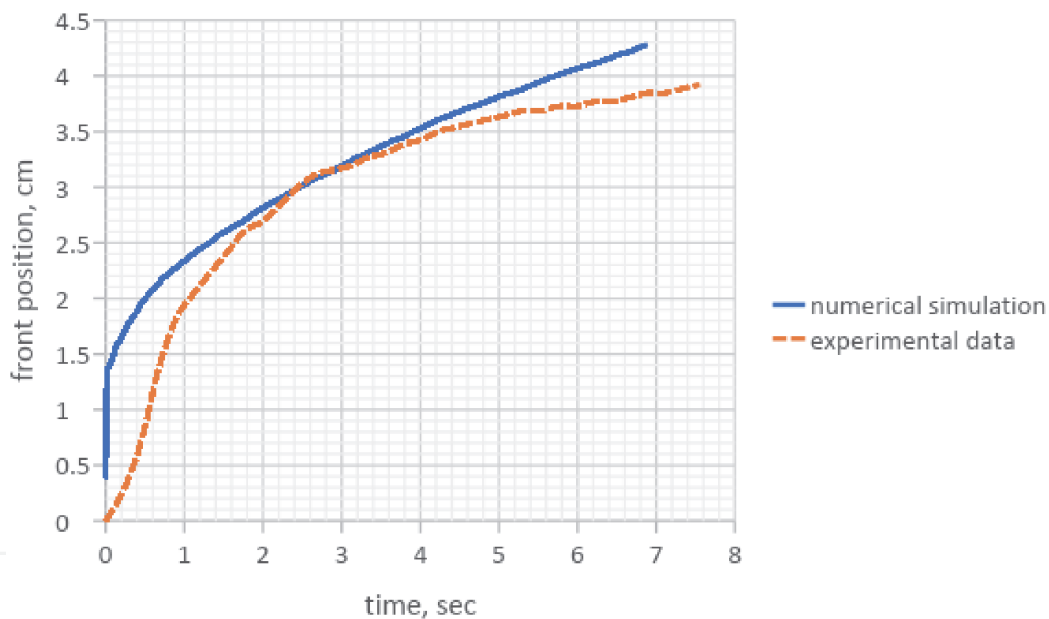


Figure 4.
 The position of the interface as a function of time for a flow in a homogeneous medium (permeability: $8.5 \cdot 10^{-9} \text{ m}^2$; porosity: 0.458; displacing fluid: viscosity: $1 \cdot 10^{-3} \text{ Pa}\cdot\text{s}$, density: 10^3 kg/m^3 ; displaced gas viscosity: $1.5 \cdot 10^{-5} \text{ Pa}\cdot\text{s}$, density: 1.4 kg/m^3 ; surface tension: 0.0582 N/m).

In the second experiment, the lower layer of the medium (with a height of 4 cm) consisted of spheres with a diameter of 6 mm, and the upper layer consisted of spheres of smaller diameter (2 mm) (Figure 5). The position of the interface is shown in the graph (Figure 6). The process of imbibition is analogous to the case of a homogeneous medium until a zone of low permeability was reached. On crossing the border of high permeable and low permeable zones, the velocity of phase interface drastically increased upon entering the zone of lower permeability small sphere assembly. After a while, the interface velocity again decreased. The acceleration of the imbibition front is explained by the fact that the capillary forces in the medium consisting of small spheres were higher. Successive slowing down of the interface was due to the decrease of permeability. The effects of increasing capillary

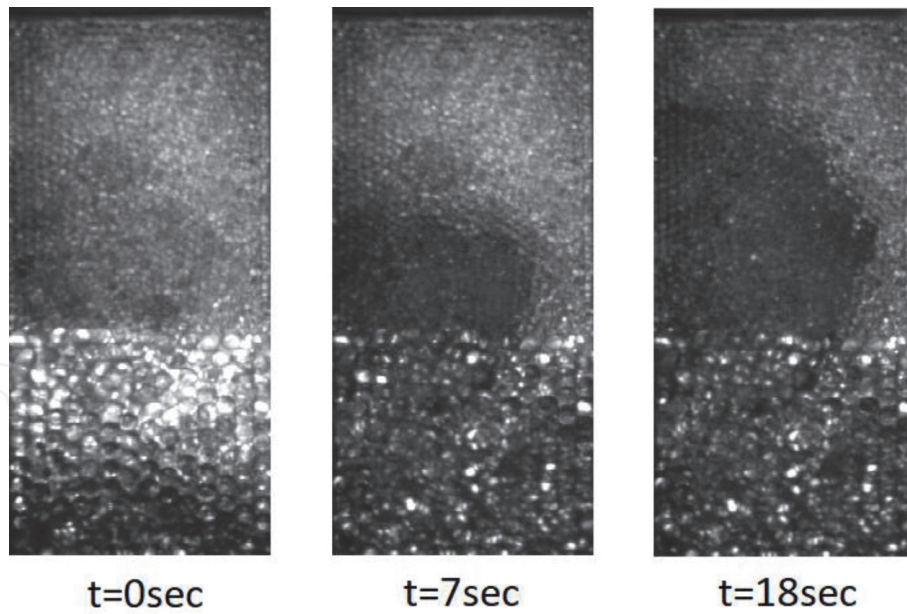


Figure 5.
 The flow of liquid in a porous medium consisting of two layers (bottom layer: height: 4 cm, permeability: $8.5 \cdot 10^{-9} \text{ m}^2$, porosity: 0.458; upper layer: permeability: $2 \cdot 10^{-9} \text{ m}^2$; porosity: 0.466) under microgravity conditions (displacing fluid: viscosity: $1 \cdot 10^{-3} \text{ Pa}\cdot\text{s}$, density: 10^3 kg/m^3 ; displaced gas: viscosity: $1.5 \cdot 10^{-5} \text{ Pa}\cdot\text{s}$, density: 1.4 kg/m^3 ; surface tension: 0.0582 N/m).

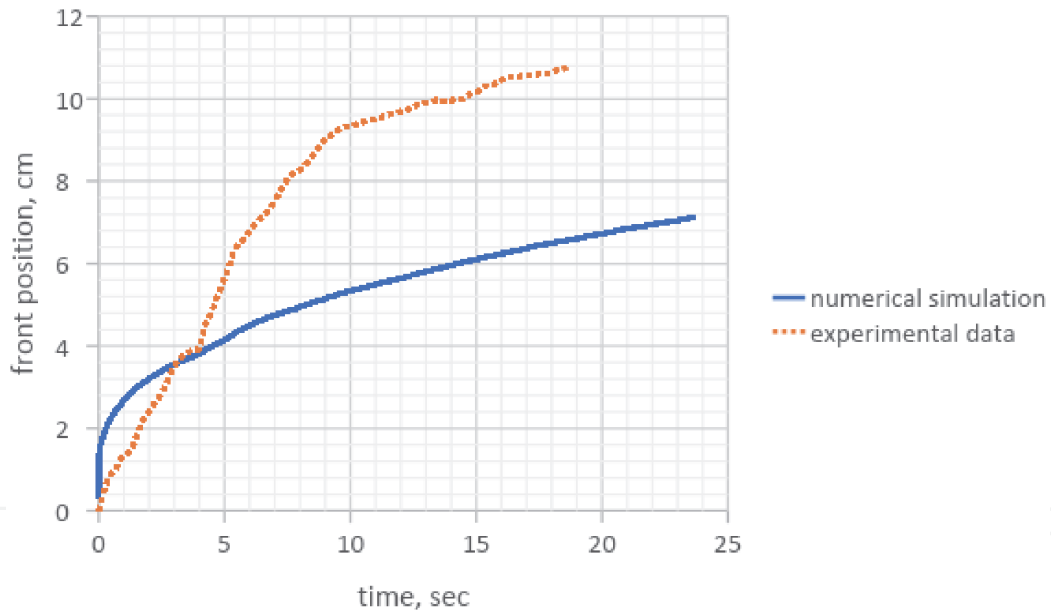


Figure 6.
 The position of the interface as a function of time for a flow in an inhomogeneous medium (bottom layer: height: 4 cm, permeability: $8.5 \cdot 10^{-9} \text{ m}^2$, porosity: 0.458; upper layer permeability: $2 \cdot 10^{-9} \text{ m}^2$, porosity: 0.466; displacing fluid: viscosity: $1 \cdot 10^{-3} \text{ Pa}\cdot\text{sec}$, density: 10^3 kg/m^3 ; displaced gas viscosity: $1.5 \cdot 10^{-5} \text{ Pa}\cdot\text{s}$, density: 1.4 kg/m^3 ; surface tension: 0.0582 N/m).

forces and drag forces acted on different time scales in unsteady-state flows: capillary forces increased by a jump, and then sustained constant value, while drag forces grew linearly on increasing the fluid penetration depth.

In the third experiment, the cell was filled with spheres ($d = 6 \text{ mm}$) and included a zone ($30 \times 20 \times 30 \text{ mm}^3$) with a lower permeability in the central part of the cell near the left wall, filled with glass beads ($d = 2 \text{ mm}$) (Figure 7). The phase interface remained relatively flat in a homogeneous zone. On approaching the zone of lower permeability, the interface becomes curved, and the capillary creeping was faster in the zone of low permeability.

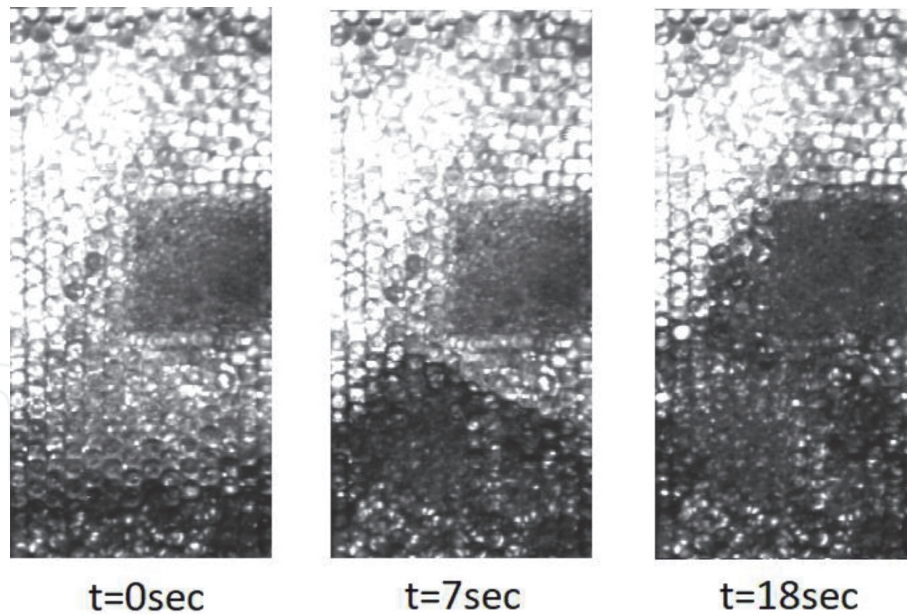


Figure 7.
 The flow of liquid in a porous medium (permeability: $8.5 \cdot 10^{-9} \text{ m}^2$; porosity: 0.458) containing an insert ($3 \times 2 \times 3 \text{ cm}^3$) with a low permeability (permeability: $2 \cdot 10^{-9} \text{ m}^2$; porosity: 0.466) under microgravity conditions (displacing fluid: viscosity: $1 \cdot 10^{-3} \text{ Pa}\cdot\text{s}$, density: 10^3 kg/m^3 ; displaced gas: viscosity: $1.5 \cdot 10^{-5} \text{ Pa}\cdot\text{s}$, density: 1.4 kg/m^3 ; surface tension: 0.0582 N/m).

3. Mathematical model and numerical investigation

This section introduces the mathematical and numerical modeling used for the experiments. A more detailed description of can be found in [16].

3.1 Balance equations

The flow of two incompressible fluids in porous media is considered, without thermal effects taken into account. The imbibition is modeled by the Darcy law, considering the capillary effects at the boundary of the phases. Non-stationarity is taken into account. Permeability and porosity depend on the spatial co-ordinate and on the fluid pressure in the pores. The mathematical formulation of the problem describes the displacement of one fluid by another due to the pressure drop on the sides of the sample or due to a given flow on one side and also due to capillary effects.

The mass balance equations for the phases are as follows:

$$\frac{\partial}{\partial t} (\varphi \rho_k s_k) + \frac{\partial}{\partial x_j} (\rho_k u_{k,j}) = 0 \quad (1)$$

Here, φ is the porosity, ρ_k is the intrinsic density of the k th phase, s_k is the phase saturation, t is the time, $u_{k,j}$ is the j th component of the seepage velocity of the k th phase, and x_j is the component of the radius vector (point coordinates). The equations are summed up over the repeated index j .

Note that the intrinsic phase velocity $v_{k,j}$ is expressed through the seepage velocity as:

$$v_{k,j} = \frac{u_{k,j}}{\varphi s_k} \quad (2)$$

Unlike the seepage velocity of a phase, intrinsic phase velocity is not determined where there is no phase (the seepage velocity at that place is zero).

Both fluids are incompressible. Dividing Eq. (1) by ρ_k yields the reduced form:

$$\frac{\partial}{\partial t}(\varphi s_k) + \frac{\partial u_{k,j}}{\partial x_j} = 0 \quad (3)$$

The average volume seepage velocity u_j is defined as:

$$u_j = u_{1,j} + u_{2,j} \quad (4)$$

Summation of the Eq. (3) using the definitions (4) leads to an equation for the total phase seepage velocity:

$$\frac{\partial \varphi}{\partial t} + \frac{\partial u_j}{\partial x_j} = 0 \quad (5)$$

In the case of porosity not changing with time, the Eq. (5) reduces to the condition of the solenoidality of the fluid seepage velocity field:

$$\frac{\partial u_j}{\partial x_j} = 0 \quad (6)$$

The momentum equations from which the Darcy laws for each phase are derived are as follows:

$$\frac{\partial}{\partial t}(\rho_k \varphi s_k v_{k,j}) + \frac{\partial}{\partial x_j}(\rho_k \varphi s_k v_{k,i} v_{k,j}) + \varphi s_k \frac{\partial p_k}{\partial x_j} = -\frac{\mu_k}{K_0} v_{k,i} + F_k \quad (7)$$

where μ_k is the dynamic viscosity, K_0 is the absolute permeability, p_k is the pressure in the phase, and F_k is the interaction force with other phases of the fluid. The right-hand side of (7) corresponds to the sum of the force of interaction with the skeleton or solid phase and the forces of interaction with other phases of the fluid.

To obtain Darcy equations, the inertial terms (i.e., non-stationary term $\frac{\partial}{\partial t}(\rho_k \varphi s_k v_{k,j})$ and convective term $\frac{\partial}{\partial x_j}(\rho_k \varphi s_k v_{k,i} v_{k,j})$) are usually neglected in (7), and the interaction forces with other phases, except the skeleton or solid phase), are modeled by modifying the basic interaction force with the skeleton by introducing relative permeability. We will neglect only the convective component of inertia, leaving the non-stationary component. After this, the Darcy equations are modified, containing the time derivative of the velocity:

$$u_{k,i} = -\frac{K_0 K_k^R}{\mu_k} \left(\frac{\partial p_k}{\partial x_i} + \frac{\rho_k}{\varphi s_k} \frac{\partial u_{k,i}}{\partial t} \right) \quad (8)$$

We assume the relative permeability of the phase, depending on its saturation s_k and, in general, on the saturation of other phases: $K_k^R = \theta_k \cdot s_k$, where θ_k is a proportionality coefficient. It should be noted that since the relative permeability is zero in the case of zero phase saturation s_k , the singularity in this case in (8) has no place. So the modified Darcy equations can be written as follows:

$$u_{k,i} + \frac{K_0 \rho_k}{\varphi \mu_k} \cdot \theta_k \frac{\partial u_{k,i}}{\partial t} = -\frac{K_0 K_k^R}{\mu_k} \frac{\partial p_k}{\partial x_i} \quad (9)$$

Denote the parameter, which is in front of the time derivative of the velocity and has the dimension of time, as T_k ; in general, it depends on its position in space, as

does absolute permeability, but not on the current distribution of variable parameters (saturation, velocity, etc.):

$$T_k = \frac{K_0 \rho_k}{\varphi \mu_k} \quad (10)$$

The Darcy equation is then written in the following form:

$$u_{k,i} + T_k \frac{K_k^R}{s_k} \frac{\partial u_{k,i}}{\partial t} = - \frac{K_0 K_k^R}{\mu_k} \frac{\partial p_k}{\partial x_i} \quad (11)$$

The parameter T_k can be called the characteristic inertia time. In the case of permeability K_0 being sufficiently small, as in ordinary porous media, this time is negligible and inertia can be neglected. But if the porous medium consists of stones/balls with a sufficiently large diameter, then such a time for low-viscosity liquids can be several seconds or more; it will most likely be impossible to neglect inertia.

Locally, the pressure difference between the phases is determined by capillary pressure, which depends only on the phase saturation, besides the skeleton data and physical data of the surface separating the phases. Hereinafter, we assume that there are only two fluid phases in the pore space, so that:

$$p_1^c(s_1) = p_2 - p_1 = -p_2^c(s_2), \quad s_1 + s_2 = 1 \quad (12)$$

3.2 Modeling relative permeability and capillary pressure

The relative permeabilities K_k^R are calculated using the Brooks-Cory model [17]:

$$K_k^R = \begin{cases} k_k^0 S_k^{n_k^0}, & s_k \geq s_k^{res} \\ 0, & s_k < s_k^{res} \end{cases}, \quad S_k = \frac{s_k - s_k^{res}}{1 - s_1^{res} - s_2^{res}} \quad (13)$$

Here, $k_k^0 > 0$ and $n_k^0 > 0$ are the model parameters, and the effective saturation S_k is determined by the residual saturations of $0 \leq s_k^{res} \leq 1$ ($s_1^{res} + s_2^{res} < 1$). It should be noted that for $0 \leq S_k \leq 1$, a porous medium is impregnated with both fluids; the phase saturation at $s_k \leq s_k^{res}$ is not described with this model. Further, we always assume that impregnation with both fluids takes place, and under these conditions, the zero alternative of (13) can be disregarded. It can also be noted that $S_2 = 1 - S_1$, and thus index 1 is omitted further and at reduced saturation, the effective saturation of the second phase is expressed through the first. For the effective saturation and relative mobility of the phases not based on the model (13) and definition (14), we have the following expressions:

$$\begin{cases} S_k = \frac{s_k - s_k^{res}}{1 - s_1^{res} - s_2^{res}} \\ M_1 = \frac{k_1^0}{\mu_1} S_1^{n_1^0} \\ M_2 = \frac{k_2^0}{\mu_2} (1 - S)^{n_2^0} \end{cases} \quad (14)$$

Capillary pressure from the k th phase is expressed through the J-function of Leverett [1] and some other parameters like:

$$p_k^c = \frac{\sigma \cos \alpha_k}{\sqrt{K/\varphi}} J(s_k) \quad (15)$$

where σ is the coefficient of surface tension, and α_k is the angle between the wall from the phase k and the interface (wetting angle). If this angle is less than $\pi/2$, then the phase is wetting; if not, it is nonwetting.

Suppose the definition (15) holds for both phases with the same J-function. In this case, (12) leads to:

$$\cos \alpha_k J(s_k) = -\cos \alpha_{k'} J(s_{k'}) = \cos \alpha_k J(1 - s_k)$$

where the primes refer to nonwetting phase and, because of the connection between the wetting angles, we get

$$J(s) = J(1 - s) \quad (16)$$

None of the known models of the Leverett function imply the right side of (16). Consequently, the expression (15) should be considered only for one of the phases, but from the side of the other phase, the capillary pressure is determined by (12). In most of models, a wetting phase k ($\alpha_k < \pi/2$) is modeled using (15), while the nonwetting phase k' makes an adjustment to the definition of capillary pressure:

$$p_{k'}^c = \frac{\sigma \cos \alpha_{k'}}{\sqrt{K/\varphi}} J(s_k) \quad (17)$$

Using both expressions (15) for the wetting phase and (17) for the nonwetting, we express the capillary pressure using data from phase 1 (omitting the index 1 of capillary pressure, wetting angle, and saturation):

$$p^c = \frac{\sigma \cos \alpha}{\sqrt{K/\varphi}} \cdot \begin{cases} J(s), & \alpha \leq \pi/2 \\ J(1 - s), & \alpha > \pi/2 \end{cases} \quad (18)$$

Let the J-function of Leverett be modeled by two parameters $C_J > 0$ and $a_J > 0$ and effective saturation:

$$J(s_k) = C_J S_k^{-a_J}, \quad \alpha_k \leq \pi/2 \quad (19)$$

Boundary conditions used:

At the inflow $z = 0$, we set the pressure $p = p_{in}$ and maximal saturation $s = 1 - s_{res}^2$.

At the outflow, we set a zero pressure and zero saturation normal derivative.

At the impermeable walls, we set to zero the normal components of phase velocities $u_{kn} = 0$, and this corresponds to zero normal derivatives of pressure and saturation.

To demonstrate the role of inertial effects in this problem, two calculations are carried out: with and without inertia (**Figure 8**). It is seen that the dynamics of imbibition on the left and right graphs are significantly different. When inertial effects are taken into account (left side), the graph has first a shape of a quadratic function of time (0–0.02 s), then linear (0.02–0.06 s), and then as a square root (0.06–2 s). When approaching zones with different permeability, these shape sections repeat: quadratic (2–3 s), linear (3–3.9 s), and square root. This result is consistent with the results presented in [7]. When inertial effects are not taken into account (right), the graph has the form of a monotonously increasing function close to a square root with a small break when passing through the border of zones with different permeability (4 cm).

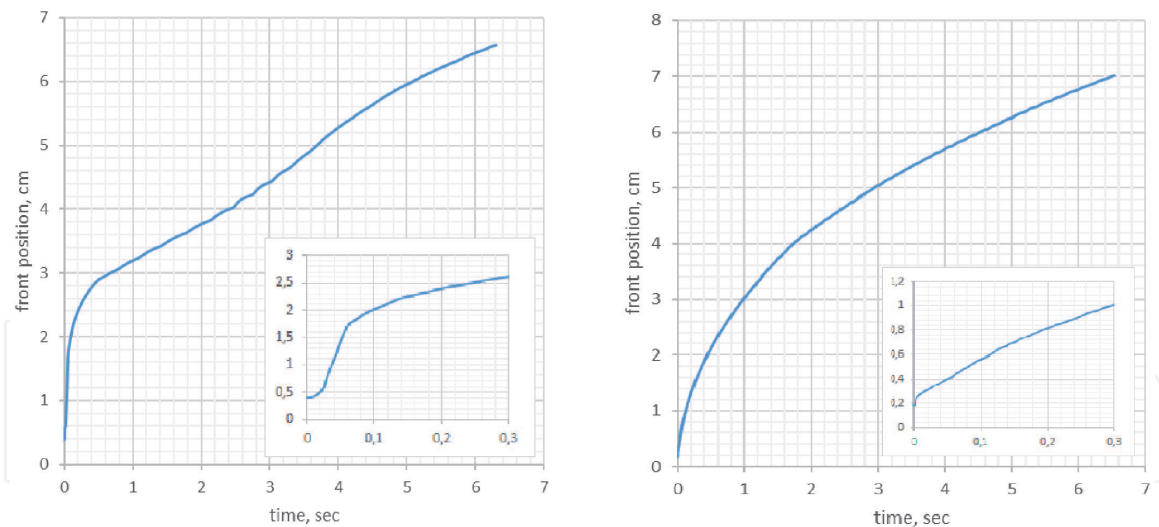


Figure 8.
 Positions of the interface as a function of time for a flow in an inhomogeneous medium with inclusion of inertia (left) and excluding inertia (right) (bottom layer: height: 4 cm, permeability: $8.5 \cdot 10^{-8} \text{ m}^2$, porosity: 0.45; upper layer: permeability: $2 \cdot 10^{-8} \text{ m}^2$, porosity is 0.45; displacing fluid: viscosity: $1 \cdot 10^{-3} \text{ Pa}\cdot\text{s}$, density: 10^3 kg/m^3 ; displaced gas: viscosity: $1.5 \cdot 10^{-5} \text{ Pa}\cdot\text{s}$, density: 1.4 kg/m^3 ; surface tension: 0.0582 N/m).

4. Comparison of numerical calculations with experimental data

The microgravity quality was poor for the present experiments that does not permit us to perform quantitative comparison of results with the outcomes of numerical modeling, which were carried out for ideal conditions. Nevertheless, the qualitative results of the calculations are similar to the experiment.

In the case of flow in a homogeneous medium (**Figure 4**), the displacement is uniform gradually slowing down. In the experiment, the speed falls down more than in calculations. This is because the mathematical model does not take into account the acceleration of gravity g , which is close to zero in the experiment, but not equal to zero.

In the case of an inhomogeneous medium (**Figure 6**), when crossing the border of zones with different permeability, the graph has a complex space-time

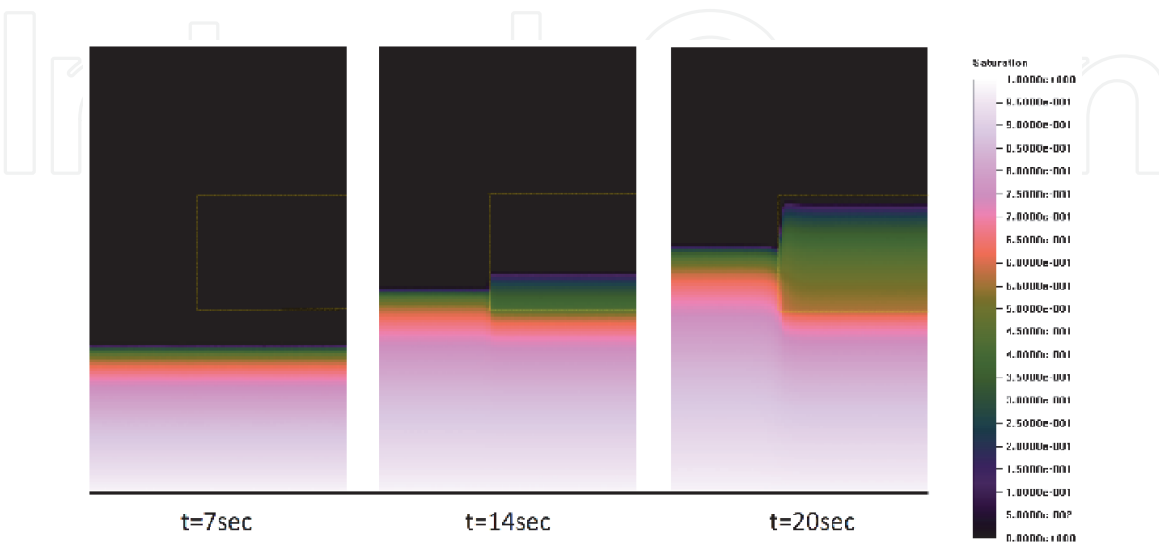


Figure 9.
 The result of numerical modeling of fluid flow in the region containing an insert with a low permeability (media permeability: $8.5 \cdot 10^{-9} \text{ m}^2$, porosity: 0.458; insert: dimensions: $3 \times 2 \times 3 \text{ cm}^3$, permeability: $2 \cdot 10^{-9} \text{ m}^2$, porosity: 0.466; displacing fluid: viscosity: $1 \cdot 10^{-3} \text{ Pa}\cdot\text{s}$, density: 10^3 kg/m^3 ; displaced gas: viscosity: $1.5 \cdot 10^{-5} \text{ Pa}\cdot\text{s}$, density: 1.4 kg/m^3 ; surface tension: 0.0582 N/m).

dependence form: quadratic (3–4.5 s), linear (4.5–5.5 s), then as square root. The main characteristic feature of the imbibition front passing through the boundary of media is its rapid acceleration (, it moves faster than if the medium were uniform, as in **Figure 4**). This corresponds to the results of the experiment.

The distribution of the saturation of the displacing liquid at different instants for the calculation, when the region contains an insert with a low permeability, is shown in **Figure 9**. This calculation corresponds to the experiment shown in **Figure 7**. In calculation, as in the experiment, having reached the insertion, the liquid begins to flow through the insert faster than in the zone with a higher permeability. The calculation also shows that the dispersion in a less permeable medium is higher (**Figure 9**).

5. Space experiments on capillary driven imbibition

Carrying out experiments on capillary seepage in space allows observing imbibition under conditions of higher quality microgravity and for longer periods. Such experiments were described in detail in [9, 14]. Here, we give a brief description of these experiments and show the possibility of determining empirical constants in mathematical models based on experimental data.

5.1 Experiment payload

Experiments on capillary driven seepage of oil in natural porous medium (sand) were performed within the frames of the MIRROR GAS programme. The experiments were prepared and supervised by Dr. D'Arcy Hart, C-CORE (Memorial University of Newfoundland), Drs. Laurier Schramm and Fred Wassmuth, Petroleum Recovery Institute (PRI, Calgary). The MIRROR payload is shown in **Figure 10**.

Liquid seepage was observed in three sample cylinders with the same porous medium: mixture of 20% (by weight) kaolinite (a sort of clay) and 80% silica sand. The fluids moving in each of the three cells were crude oil, lubricating oil, and polymer in distilled water.

The media and fluids were transported separately into orbit. An experiment cell consisted of a reservoir and a soil cell, with a sliding gate dividing the two (see **Figure 11**). At the beginning of the experiment, the stepper motor retracted the sliding gate, exposing the soil to the reservoir fluid, whereupon the liquid began to leak under the action of capillary forces under microgravity conditions. The level of fluid in the soil was detected using 48 fiber optic sensor probes located along the length of the sample. The results of the experiment are shown in **Figure 12** (black asterisk markers).

5.2 Mathematical model for multiphase seepage

We consider the seepage of a liquid through the area of length L . The capillary forces are taken into account. The nonlinear convection-diffusion equation for a porous medium is [12, 13].

$$\varphi \frac{\partial s}{\partial t} + \frac{\partial}{\partial x} \left(F - D \frac{\partial s}{\partial x} \right) = 0, \quad (20)$$

where s is the saturation of the displacing fluid, φ is the porosity, D is the diffusion coefficient, and F is the convection flux.

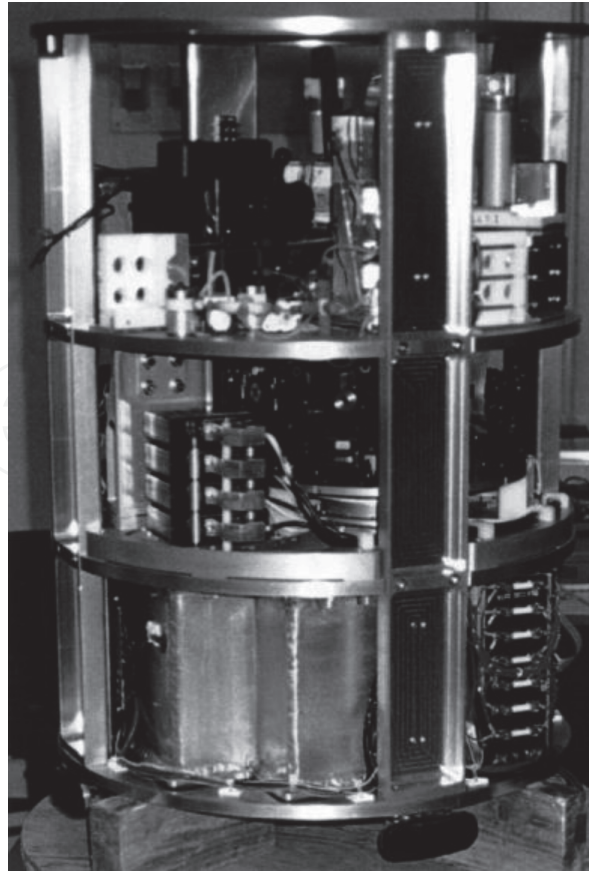


Figure 10.
 MIRROR payload ready for GAS container integration at Kennedy Space Center. Capillary flow experiment cells are in the right-hand part of the upper section.

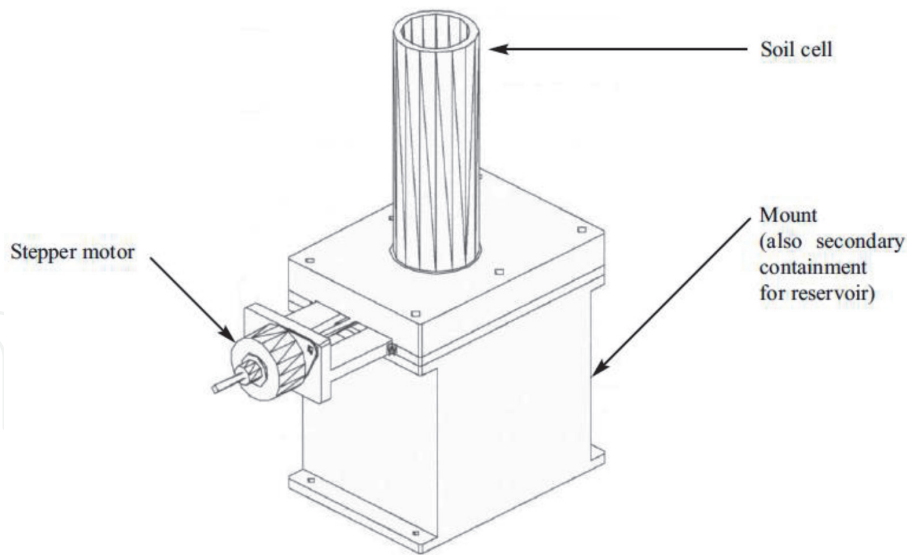


Figure 11.
 Experiment cell for space experiments on capillary driven imbibition.

The initial conditions for saturation $s(t, x)$ are

$$s(0, x) = \begin{cases} s_{max}, & x = 0; \\ s_{min}, & x > 0. \end{cases} \quad (21)$$

The boundary conditions are

$$s(t, 0) = s_{max}, \quad \left(\frac{\partial s}{\partial x} \right)_{x=L} = 0. \quad (22)$$

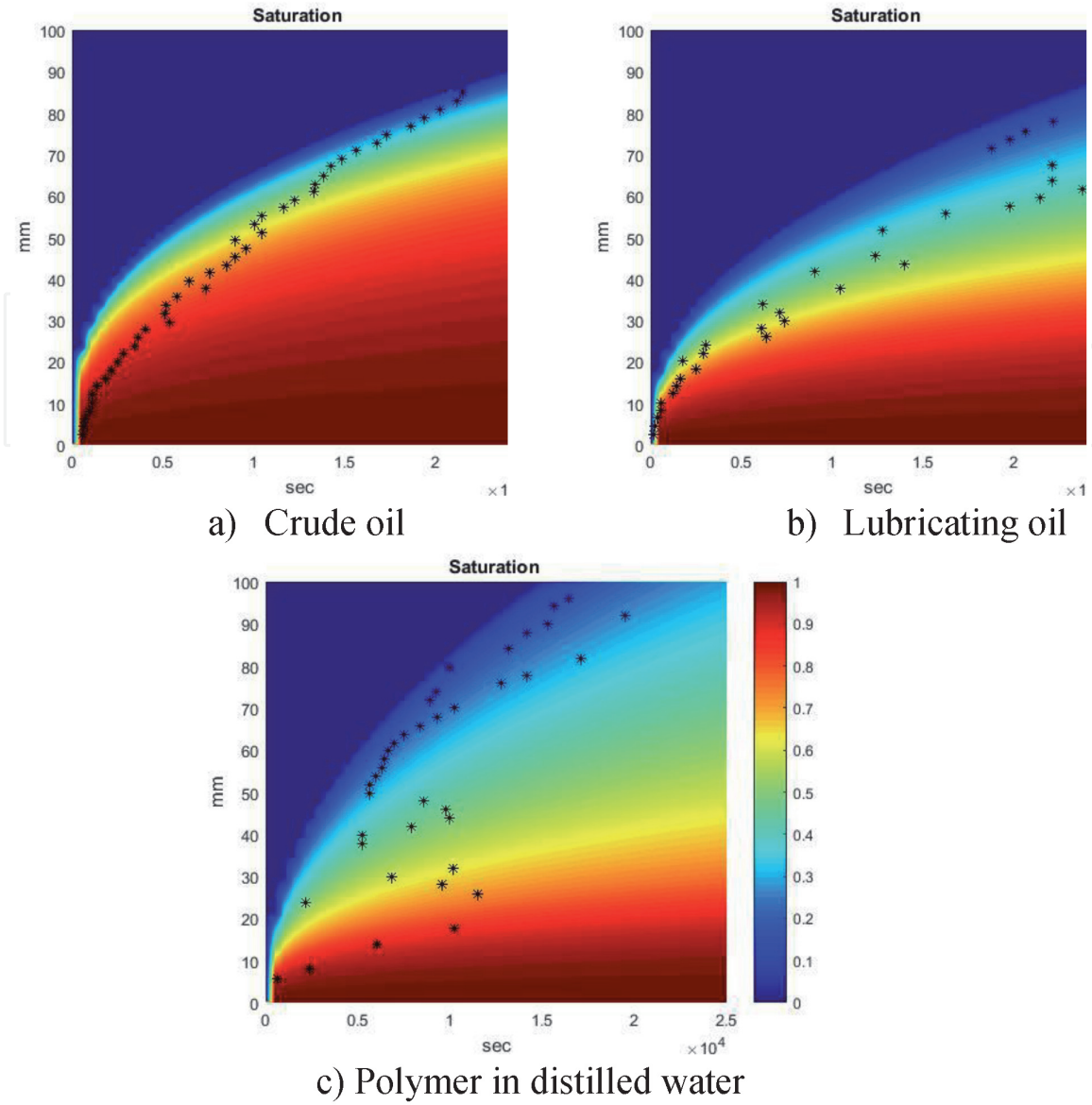


Figure 12. Results of numerical modeling of the imbibition process of a liquid into a porous medium under the influence of capillary forces compared to experiment results.

where s_{min} and s_{max} are respectively the minimum and maximum possible saturations.

The convection-diffusion equation with initial and boundary conditions describes the displacement of a quantity s propagating as a step along the x -axis from the left to the right, if the convection flux is positive ($F > 0$) [7, 8]. The diffusion coefficient D is always positive; it blurs the front of propagation.

The effective saturation S is

$$S = \frac{s - s_{min}}{s_{max} - s_{min}}. \quad (23)$$

Below, the index “O” corresponds to the displacing fluid (“oil”). The index “G” corresponds to the displaced liquid (“gas”). Dimensionless relative mobilities M_O and M_G are calculated by the Brooks and Corey model:

$$M_O = k_O S^{n_O}, \quad M_G = \frac{\mu_O}{\mu_G} k_G (1 - S)^{n_G}, \quad (24)$$

where n_O, k_O, n_G, k_G are empirical constants. When simulating two-phase seepage, the expression for F is as follows:

$$F = \tilde{F} = -\frac{KM_O}{\mu_O} \frac{\partial p}{\partial x} = \frac{M_O}{M_O + M_G} u(t) \quad (25)$$

where $u(t)$ is the total seepage velocity.

Formula (25) was obtained as a result of averaging in modeling integral parameters with the help of 1D Equation [12].

Additional effect associated with the instability of capillary affected flows is modeled by the application of an auxiliary term to F :

$$F = \tilde{F} + F_0((s - s_{min})(s_{max} - s))^\alpha = \frac{M_O}{M_O + M_G} u(t) + F_0((s - s_{min})(s_{max} - s))^\alpha. \quad (26)$$

The details of such method for 1D approximation for 3D results are discussed in [13].

This term is proportional to the empirical coefficient F_0 . It intensifies the dispersion of the displacement front. The sign of F_0 is positive since the instability intensifies the flow.

The total seepage velocity is either specified (flux control)

$$u(t) = U_0, \quad (27)$$

or calculated using a definite integral (pressure control)

$$u(t) = \frac{K\Delta P_0}{\mu_O} \left[\int_0^L \frac{dx}{M_O + M_G} \right]^{-1}. \quad (28)$$

where ΔP_0 is constant pressure drop.

The diffusion coefficient D is constructed from the sum of the diffusion coefficients due to the capillary forces d_C and the dispersion, which simulates, in the one-dimensional approximation, the blurring of the front due to other effects.

Diffusion formed by capillary forces d_C looks according to the Leverett model:

$$d_C = \frac{C_J a_J |\cos \theta| \sigma \sqrt{K\phi} M_O M_G}{\mu_O (s_{max} - s_{min}) (M_O + M_G)} \cdot \begin{cases} S^{-1-a_J}, & \cos \theta > 0; \\ (1 - S)^{-1-a_J}, & \cos \theta < 0; \end{cases} \quad (29)$$

where θ is the wettability angle on the side of the displacing liquid, and C_J, a_J are parameters of the Leverett function. Similar procedure was described in [1].

The dispersion depends on the total flux of the phase and is proportional to its magnitude. Thus, considering dispersion and capillary effects, the diffusion coefficient D is modeled [10, 11] as

$$D = d_C + \left| F - d_C \frac{\partial s}{\partial x} \right|. \quad (30)$$

We note that the additional factor which is proportional to the coefficient F_0 also enters into the dispersion structure.

Processing the mathematical model described above makes it possible to select the coefficients responsible for the blurring of the front on the basis of experimental data. We have obtained that for the three experiments described above, the optimal coefficients are as follows (**Table 1**):

| | C_J | a_J | F_0 |
|----------------------------|-------------------|-------|---------------------|
| Crude oil | $3 \cdot 10^{-2}$ | 0.5 | $3 \cdot 10^{-8}$ |
| Lubricating oil | $1 \cdot 10^{-2}$ | 0.5 | $1.5 \cdot 10^{-7}$ |
| Polymer in distilled water | $5 \cdot 10^{-3}$ | 0.5 | $4.5 \cdot 10^{-7}$ |

Table 1.
Optimal coefficients for the three experiments.

The pressure drop or the specified flux was absent, so that the motion was carried out only by capillary forces.

The distribution of the saturation of the penetrating liquid in the calculated region over time is shown in **Figure 12**. The parameters of each of the three calculations corresponded to the actual experiment. The experimental data are marked with black asterisk markers.

Thus, as can be seen from **Figure 12**, the results of numerical calculations based on the proposed mathematical model are in good agreement with the experimental data. The blurring of the displacement front for each of the liquids is different: the smallest blurring is observed in crude oil (**Figure 12(a)**), and the front is most strongly blurred in the case of imbibition of polymer (**Figure 12(c)**). For each fluid, the empirical constants C_J , a_J , and F_0 are selected. The value of a_J for all liquids is chosen to be 0.5. The coefficients C_J and F_0 are different for each case, but they are of the same order. The coefficients were chosen in such a way that the blurring of the front in the numerical calculation would have the least difference from the experimental data.

6. Conclusions

Experiments on the imbibition of a fluid into an inhomogeneous artificial porous medium under microgravity conditions during parabolic flights are considered. A mathematical model for multiphase seepage considering inertial effects is developed. The results of the experiment are compared with the results of numerical simulation of the flow of a viscous liquid in a porous medium, taking into account capillary and inertial effects. It is shown that when the transition from a more permeable medium to a less permeable one takes place, the velocity of the imbibition front increases. This is because the capillary forces in a medium with a low permeability are larger. On further imbibition into the low permeable medium, the velocity of imbibition decreases much faster than that in highly permeable medium. It is also shown that the dispersion of fluid during its imbibition into a less permeable medium is much higher. A model describing the displacement front blur due to diffusion, capillary effects, and flux instability was developed; the model uses two empirical constants. This model can describe the displacement front peculiarities even in 1D problem setup. To estimate those empirical constants, the results of experiments in microgravity were used; those conditions were needed to exclude the gravity factor affecting the flux and diminishing the capillary effects.

Acknowledgements

Authors express warmest gratitude and high appreciations of the results by Professor Jean Claude Legros, who was initiator and principle investigator in these researches. The experimental hardware and methodology were developed by

Dr. Eric Istasse and became the base of his thesis [15]. The authors with financial support of Russian Academy of Sciences performed theoretical investigations and numerical simulations.

IntechOpen

Author details

Nikolay Smirnov^{1,2}, Valeriy Nikitin^{1,2} and Evgeniya Kolenkina (Skryleva)^{1,2*}

1 Moscow M.V. Lomonosov State University, Moscow, Russia

2 Scientific Research Institute for System Analysis of the Russian Academy of Sciences, Moscow, Russia

*Address all correspondence to: jennyne@yandex.ru

IntechOpen

© 2020 The Author(s). Licensee IntechOpen. This chapter is distributed under the terms of the Creative Commons Attribution License (<http://creativecommons.org/licenses/by/3.0>), which permits unrestricted use, distribution, and reproduction in any medium, provided the original work is properly cited. 

References

- [1] Barenblatt GI, Entov VM, Ryzhik VM. Theory of Fluids Flows through Natural Rocks. Dordrecht, Boston, London: Kluwer Academic Publishers; 1990
- [2] Bear J, Bachmat Y. Introduction to Modelling of Transport Phenomena in Porous Media. Dordrecht, Boston, London: Kluwer Academic Publishers; 1990
- [3] Bear J. Dynamics of Fluids in Porous Media. New York: Dover Publications Inc.; 1988
- [4] Kaviany M. Principles of Heat Transfer in Porous Media. 2nd ed. New York: Springer-Verlag; 1995
- [5] Nield DA, Bejan A. Convection in Porous Media. New York/Berlin/Heidelberg/London: Springer-Verlag; 1992
- [6] Nigmatilin RI. Dynamics of Multiphase Media. Moscow Science Publication; 1987
- [7] Smirnov NN, Dushin VR, Legros JC, Istasse E, Boseret N, Mincke JC, et al. Multiphase flows in porous medium—Mathematical model and microgravity experiments. *Microgravity Science and Technology*. 1996;**IX/3**:222-231
- [8] Smirnov NN, Nikitin VF, Norkin AV, Kudryavtseva OV, Legros JC, Istasse E, et al. Capillary driven filtration in porous media. *Microgravity Science and Technology*. Hanser Publications, Munich, Germany. 1999;**XII/1**:23-35
- [9] Smirnov NN, Legros JC, Nikitin VF, Istasse E, Schramm L, Wassmuth F, et al. Filtration in artificial porous media and natural sands under microgravity conditions. *Microgravity Science and Technology*. Bremen, Germany: Z-Tec Publishing. 2003;**XIV/2**:3-28
- [10] Smirnov NN, Nikitin VF, Ivashnyov OE, Maximenko A, Thiercelin M, Vedernikov A, et al. Microgravity investigations of instability and mixing flux in frontal displacement of fluids. *Microgravity Science and Technology*. 2004;**XV/3**: 3-28
- [11] Smirnov NN, Dushin V, Nikitin V, Philippov Y. Two phase flows in porous media under microgravity conditions. *Microgravity Science and Technology*. 2008;**20**(3–4):155-160
- [12] Smirnov NN, Dushin VR, Nikitin VF, Philippov YG, Nerchenko VA. Three-dimensional convection and unstable displacement of viscous fluids from strongly encumbered space. *Acta Astronautica*. 2010;**66**:844-863
- [13] Smirnov NN, Nikitin VF, Maximenko A, Thiercelin M, Legros JC. Instability and mixing flux in frontal displacement of viscous fluids from porous media. *Physics of Fluids*. 2005; **17**:084102
- [14] Dushin VR, Nikitin VF, Smirnov NN, Skryleva EI, Tyurenkova VV. Microgravity investigation of capillary driven imbibition. *Microgravity Science and Technology*. Springer. 2018;**30**(4): 393-398
- [15] Istasse E. Determination of capillary characteristics in porous media, Free University of Brussels, Faculty of Applied Sciences, Dissertation presented by Eric Istasse with a view to obtaining the Diploma of Advanced Studies in Applied Sciences, Director: Prof. Legros J.C., Academic Year 2000-2001, Brussels. 2001
- [16] Smirnov NN, Nikitin VF, Skryleva EI. Microgravity investigation

of seepage flows in porous media.
Microgravity Science and Technology.
Springer. 2019;31(5):629-639. DOI:
10.1007/s12217-019-09733-7

[17] Larry WL. Enhanced Oil Recovery.
Englewood Cliffs, New Jersey: Prentice-
Hall; 1989

IntechOpen

IntechOpen